# Numerical prediction of temperature and density distributions in selective laser sintering processes

*Gabriel Bugeda Miguel Cervera and Guillermo Lombera*

## The authors

**Gabriel Bugeda** and **Miguel Cervera** are both with the Civil Engineering Department at the Technical University of Catalonia (UPC), Barcelona, Spain.
**Guillermo Lombera** is at the National Institute of Materials Technology, National University of Mar del Plata, Mar del Plata, Argentina.

## Keywords

Finite elements, Numerical analysis, Numerical simulation, Rapid prototyping, Selective laser sintering

## Abstract

A finite element model has been developed for the 3D simulation of the sintering of a single track during a selective laser sintering process (SLS). The model takes into account both the thermal and the sintering phenomena involved in the process. Owing to the continuous movement of the laser beam the model takes also into account the transient nature of the problem. This is transformed into a pseudo-static one through a transformation of the coordinates system of the equations. Nevertheless, this transformation introduces a convective term into the heat equations that produces instabilities in the solution. These instabilities have been solved by using a stream upwind Petrov Galerkin (SUPG) strategy together with a shock capturing scheme. Finally, a fixed point strategy is used for the solution of the analysis. The model has been tested through the solution of some examples.

## Introduction

Selective laser sintering (SLS) is a manufacturing technique which uses a laser beam to sinter material powder in a selective way to produce three dimensional parts. This technique was initially developed at the University of Texas at Austin, and by the companies DTM Corporation, Austin, Texas and BFGoodrich, Brecksville, Ohio. This process consists of three stages (Scherer, 1977a; 1977b; 1977c; 1986) as it is schematized in Figure 1:

(1) A layer of powder is deposited on the elevator and pressed; each layer of powder is pre-heated before the scanning to minimize the need of induced laser heat.
(2) Laser radiation sinters the powder to form the profile of the section.
(3) The elevator drops through a distance equivalent to the thickness of the section, and the process is repeated until the prototype is completed.

The materials employed are nylon, polycarbonate, ABS, and metal powders. The physical processes associated to this technology include heat transfer and sintering of powder (Ming-Shen *et al.*, 1991a; 1991b; Weissman and Hsu, 1991). The sintering models used in this work are based on the analysis of Scherer (1977a; 1997b; 1977c; 1986) and Mackenzie and Shuttleworth (1949). In this analysis, the temperature at each point of the powder bed provides the sintering rate, and the density change is obtained by integration of the sintering rate. Also, the thermal conductivity at each point of the particle bed is a function of the density.

In addition to the thermal and sintering models used in this work there are other possibilities like the models presented by Berzins *et al.* (1996) and Williams and Deckard (1998). These alternative models could also be integrated in the coupled solution strategy presented at the end of this work.

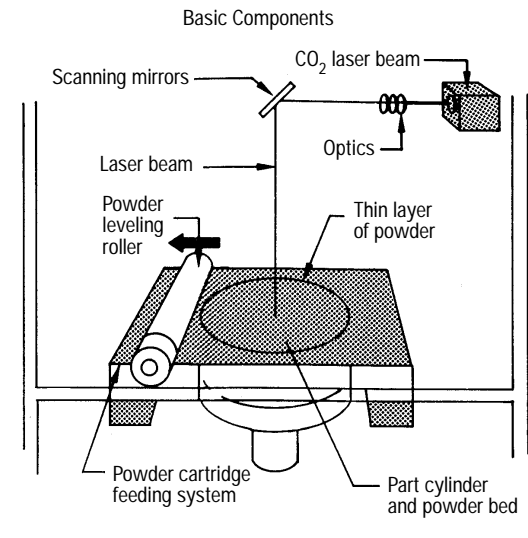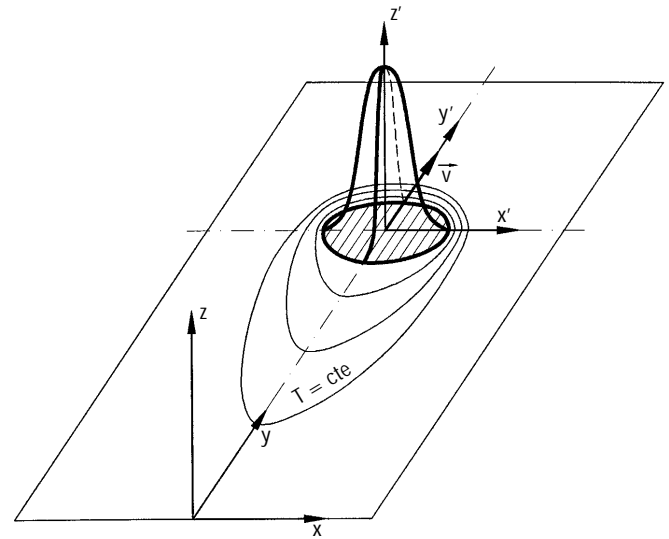**Figure 1** Selective laser sintering system



**Figure 2** Thermal model



## Thermal submodel

The heat transfer behavior in the powder bed can be described by the classical conduction equation:

$$\rho c \frac{\partial T}{\partial t} = \nabla(k_e \nabla T) + g(x, y, z, t) \qquad (1)$$

where $p, c, k_e$ are the apparent density, specific heat of the full dense solid material and effective thermal conductivity of the powder bed, respectively, and $g(x, y, z, t)$ is an internal heat source function.

In contrast to the conduction problem of a solid material, the thermal conductivity of a powder bed can vary from point to point depending on the local temperature as well as the condition of contact between particles and the local porosity. Yagui and Kunni (1989) have formulated a model for the effective conductivity of a packed bed considering the conduction, convection and radiation effects within a powder bed:

$$k_e = \frac{\mu k_s}{1 + \Phi \dfrac{k_s}{k_g}} \qquad (2)$$

where $k_s$ is the conductivity of the solid material, $k_g$ is the conductivity of air, $\mu$ is the solid fraction $\mu = \frac{\rho}{\rho_s}$ (where $\rho_s$ is the density of the solid material) and $\Phi$ is an empirical coefficient normally taken as $\Phi = 0.02 \times 10^{2(0.7-\mu)}$. Expression (2) allows to compute the real conductivity at each point of the problem in terms of the powder density.

The thermal problem to be solved with equation (1) is schematized in Figure 2. There is a laser beam that moves in the $y$ direction with a constant velocity $v$. Owing to

the movement of the laser beam this is a transient problem. Nevertheless, it can be transformed into a steady problem with a change in the coordinate axes of the problem. This change consists of using a local coordinate system centered at the laser beam. The new system of coordinates is the following:

$$\begin{cases} x' \equiv x \\ y' \equiv y - vt \\ z' \equiv z \\ t' \equiv t \end{cases} \qquad (3)$$

Then equation (1) can be rewritten in terms of the new coordinates system as:

$$\rho c \frac{\partial T}{\partial y'} = \nabla(k_e \nabla T) + g(x', y', z') \qquad (4)$$

From the mathematical point of view the main difference between equation (1) and equation (4) is that the last one does not contain any dependence with respect to the time variable $t$ but, on the other side, a new convective term appears at the left side of the equality. This type of term produces some additional difficulties.

In order to solve equation (4) the domain indicated in Figure 1 has been defined. Following the notation of Figure 1 and using $\boldsymbol{n}$ for the vector normal to a boundary and $\boldsymbol{q}$ for the thermal flux ($\boldsymbol{q} = k_e \nabla T$) the boundary conditions that have been applied for the resolution of equation (1) are the following:
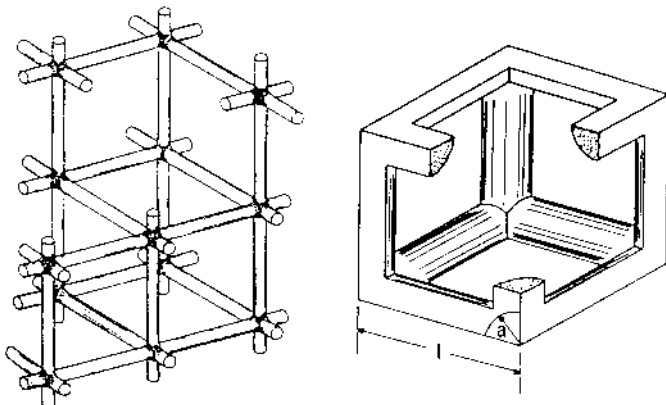- Symmetry plane condition for $x' = 0$ ($\boldsymbol{n}^t \boldsymbol{q} = 0$).

- Local temperature equal to the external temperature ($T = T_e$) at $x' = w$, $y' = L_1$ and $z' = -d$.
- Convection-radiation condition at $z' = 0$: $\mathbf{n}^t\mathbf{q} = -\alpha(T - T_e)$ being $\alpha$ the convection-diffusion coefficient.
- Thermal flux equal at the laser beam intensity ($\mathbf{n}^t\mathbf{q} = I$) at the incidence zone.
- Owing to the fact that both the temperature and the thermal flux are unknown at $y' = -L_2$ unless this part of the boundary be very far away from the laser beam no boundary condition has been applied there. From the mathematical point of view this is an unusual type of boundary condition. Additional information about this type of boundary condition can be found in (Papanastasiou *et al.*, 1992).

## Sintering submodel

To follow the evolution of the density (or void fraction) as a function of time and temperature, the Scherer (1977a; 1997b; 1977c; 1986) and the Mackenzie and Shuttleworth (1949) models have been used. Both of these models assume that the surface energy reduction of the sintering powder drives the process through viscous mass flow dissipation. In the lower density range (i.e. $\rho \leq 0.94\rho_s$) the Scherer model assumes that the powder consists of an open pore network of cylinders arranged cubically, with the cylinder diameters equal to the particle diameter and the cylinder lengths proportional to the pore diameter (see Figure 3). As sintering proceeds, the cylinder heights collapse, reducing the void fraction in the powder bed, until the cylinder walls touch each other. At this point the Mackenzie-Shuttleworth model describes the powder bed by contiguous spheres with closed pores (see Figure 4).

The essential relationships for both models describe the free strain rate $\frac{\partial e}{\partial t}$ of the sintering material as follows:

$$\frac{\partial e}{\partial t} = -\frac{M}{\eta}\frac{(3\pi)^{1/3}}{6}\frac{2 - 3dX}{\sqrt[3]{X(1 - dX)^2}} \tag{5}$$

for open pore, low density powder beds and partially sintered parts (i.e. $\rho \leq 0.94\rho_s$) where $X$ is the cylinder aspect ratio (Scherer model), and
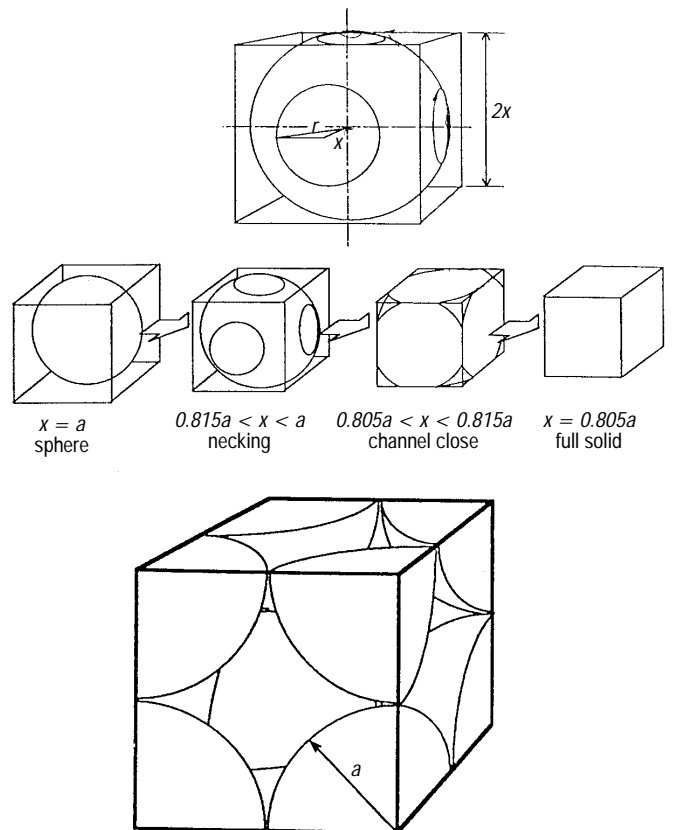
$$\frac{\partial e}{\partial t} = -\frac{M}{\eta}\frac{1}{2}\frac{(4\pi)^{1/3}}{3}\left(\frac{\rho_s}{\rho} - 1\right)^{2/3} \tag{6}$$

for closed pore beds (i.e. $\rho > 0.94\rho_s$) and solid parts (Mackenzie-Shuttleworth model). The quantity $M$ appearing in both equations is given by:

$$M = \gamma n^{1/3} \tag{7}$$

where $\gamma$ is the surface energy and $n$ is the number of particles per unit volume of fully densifted material. The quantity $\eta$ is the

**Figure 4** Mackenzie-Shuttleworth model for $\rho > 0.94\rho_s$: network of contiguous spheres



$x = a$
sphere

$0.815a < x < a$
necking

$0.805a < x < 0.815a$
channel close

$x = 0.805a$
full solid

**Figure 3** Scherer model for $\rho \leq 0.94\rho_s$: open pore network of cylinders arranged cubically

viscosity of the material, which is an Arrhenius-type function of temperature, given by:

$$\eta = \eta_0 exp\left(\frac{\Delta E}{RT}\right) \qquad (8)$$

where $\eta_0$ is the viscosity coefficient and $\Delta E$ is the activation energy. The strain rate for low density sintering is also seen to be a function of $X$. This is the aspect ratio of the cylinders that make up the unit cell in that model. The constant $d$ in equation (5) is $8\sqrt{2}/3\pi$. In the Mackenzie-Shuttleworth model, the strain rate is a function of the ratio of the densities of the fully sintered material $\rho_s$ and the actual density of the bed $\rho$.

As the particles sinter, the void fraction $\varepsilon$ drops. The Scherer model gives an expression for $\varepsilon$ as a function of the cylinder aspect ratio in the unit cell as:

$$\varepsilon = 1 - 3\pi X^2 + 8\sqrt{2}X^3 = 1 - \frac{\rho}{\rho_s}$$

$$= 1 - \frac{\rho_0}{\rho_s} exp(-3e) \qquad (9)$$

Given a value of the particle bed density or void fraction, equation (9) can be used to find the corresponding value of $X$ which in turn can be substituted into equation (5) to find a new strain increment $\Delta e$.

As in the thermal model, the change in the coordinate system (3) has been implemented and equations (5) and (6) are rewritten as:

$$\begin{cases} \dfrac{\partial e}{\partial y'} = \dfrac{M}{\eta}\dfrac{(3\pi)^{1/3}}{6v}\dfrac{2-3dX}{\sqrt[3]{X(1-dX)^2}} \\ \qquad\qquad\qquad if\ \rho \le 0.94\rho_s \\ \dfrac{\partial e}{\partial y'} = \dfrac{M}{\eta}\dfrac{1}{2v}\dfrac{(4\pi)^{1/3}}{3}(\dfrac{\rho_s}{\rho}-1)^{2/3} \qquad (10) \\ \qquad\qquad\qquad if\ \rho > 0.94\rho_s \end{cases}$$

## Coupled model and solution strategy

The analysis of the sintering process involves the coupled solution of the thermal equation (4) and the sintering equations (10). Both equations are linked by the expression (2) that relates the thermal conductivity at each point with the powder bed density. The strategy for the solution of this set of coupled equations is as follows:

(1) Assuming a given distribution of thermal conductivities equation (4) is solved by using a finite element discretization. This discretization leads to a non-symmetric system of equations. A stream upwind

Petrov Galerkin (SUPG) strategy (Brooks and Hughes, 1982) together with a shock capturing scheme (Codina, 1993) are used for the elimination of the spurious oscillations produced by the first order derivative term of equation (4).

(2) The nodal temperatures obtained in (1) are used for the obtainment of a new set of nodal density values. These new values are obtained by using equations (7), (8), (9) and (10).

(3) With the new density values equation (2) is used to get new values of the thermal conductivity. The new thermal conductivity values allow to go back to step (1). This iterative process is repeated until convergence.

The necessary input data for this iterative solution process is:
- Laser beam intensity $I_o$, radius w and beam velocity $v$.
- Thermal properties: $k_s$ and $k_a$.
- Rheological properties $\mu_o$, $\Delta E$, $\eta_0$, surface tension $\gamma$.
- Geometrical variables: positions of the heat source and powder bed dimensions.
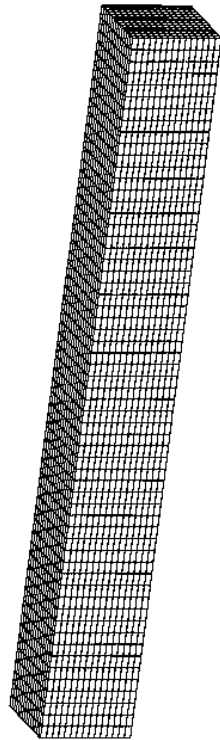
## Results and discussion

The solution strategy proposed in this paper has been validated through the analysis of the sintering process of a polycarbonate track. The initial conditions, the boundary conditions, and the material properties are shown in Table I. The finite element mesh shown in Figure 5 with 115,616 nodes and 113,500 hexahedral eight noded elements has been used for the thermal analysis. Owing to the symmetry of the problem only one half of the domain has been discretized. The dimensions of this semi-domain are $0.2cm \times 1.6cm \times 0.2cm$.

Table I Initial conditions, boundary conditions and material constants

| | |
|---|---:|
| *Initial conditions:* | |
| Initial bed temperature $T_{initial}$ (˚K) | 293 or 375 |
| Initial density $\rho_0$ ($\frac{kg}{m^3}$) | 526 |
| Initial solid fraction $\mu_0$ | 0.48 |
| | |
| *Material constants:* | |
| Full dense solid material $\rho_s$ ($\frac{kg}{m^3}$) | 1,095 |
| Viscosity coefficient $\eta_0$ (Pa.s) | $5.41x10^{-18}$ |
| Activation energy $\Delta E$ (˚K) | 20638 |
| Surface energy $\gamma$ (J/m²) | $45x10^{-5}$ |
| Particle bed specific heat $C_p$ (J/˚Kkg) | 1,580 |
| Conductivity of solid $K_s$ (W/˚K.m) | 0.21 |
| Conductivity of air $K_g$ (W/˚K.m) | 0.026 |

**Figure 5** Finite element mesh



**Figure 6** Temperature distribution for v = 50cm/s and the 200 W laser power
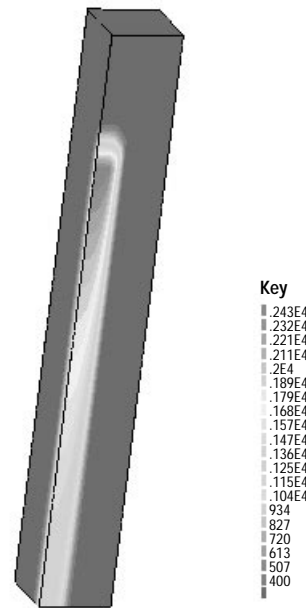


Two sets of different analyses have been defined:

(1) The first set corresponds to a case where the laser power has been fixed to $200\,W$ and the laser beam intensity $I_o$ to $1.5 \times 10^8$ $W/m^2$. Different scanning speeds have been used (0.0625, 0.125, 0.25, 0.5, 1.0, 2.0, 4.0 and 8.0 $m/s$). The initial bed temperature is $293°K$. This corresponds to a case where the initial polycarbonate powder has not been pre-heated and a high power laser beam has been used.

(2) The second set corresponds to a case where the laser power has been fixed to $10\,W$ and the laser beam intensity $I_o$ to $5.0 \times 10^7$ $W/m^2$. Different scanning speeds have been used (0.0625, 0.125, 0.25, 0.5, 1.0, 2.0, 4.0 and 8.0 $m/s$). The initial bed temperature is $375°K$. This corresponds to a case where the initial polycarbonate powder has been pre-heated and, due to that, a lower power laser beam can produce a significant amount of sintering.

The objective of both sets of analyses has been to study how the sintered depth and the density distribution change with the variation of the scanning speed while the rest of sintering parameters are maintained fixed.

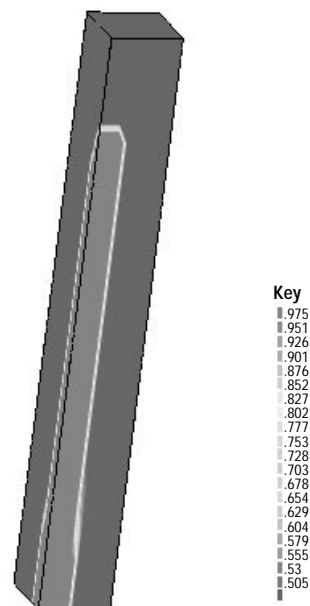Figure 6 shows the obtained temperature distribution corresponding to a scanning

speed of 0.5 $m/s$ with a laser power of 200 $W$. Temperatures range from $293°K$, which is the initial, up to $2530°K$, which is the maximum temperature just under the laser beam. Figure 6 shows how the high increase of temperature due to the laser heat is propagated in the direction of the movement of the laser beam.

Figure 7 shows the distribution of solid fraction $\mu$ in the powder bed corresponding to the same case. The values of this solid fraction range from a minimum value of 0.48, which corresponds to the initial density divided by

**Figure 7** Solid fraction distribution for v = 50cm/s and the 200 W laser power

the density of the full solid material, up to 1.0, which corresponds to the completely sintered material. There is a very good definition of the zones where the material has not started to sinter ($\mu = \mu_0 = 0.48$) and where it is completely sintered ($\mu = 1.0$). In addition, there is a very narrow band where the material is partially sintered which corresponds to solid fraction values ranging from 0.48 to 1.0.

Figure 8 shows the sintered depth obtained for each scanning speed and for both sets of analyses. It shows that for velocities higher than a specific value the sintered depth is null and no sintered material is produced. On the other side, a decrease of the scanning speed produce an increase of the sintered depth. It also shows how the pre-heating of the initial powder bed allow to get sintered tracks with a much lower laser power.

This results are in agreement with the experimental ones taken from Ming-Shen *et al.* (1991b).

## Conclusions

A three-dimensional model for selective laser sintering is derived based on the basic model structure: thermal and sintering submodels. In these models a new solution strategy has been implemented to rewrite the thermal and sintering equations in order to get a steady state problem. The resulting non-linear coupled model converges in a small number of iterations. The temperature and density distributions obtained provide useful information about the sintering properties such as the sintering depth. Future goals of this work

are to explore more experimental data on material properties to support each sub-model and to obtain the residual stresses distribution.

## References

Berzins, M., Childs, T.H.C., Dalgarno, K.W., Ryder, G.R. and Stein, G. (1996), "The selective laser sintering of polycarbonate", *Annals of CIRP*, Vol. 45 Part 1, pp. 187-90.

Brooks, A.M. and Hughes, T.J.R. (1982), "Streamline upwind/Petrov-Galerkin formulations for convection dominated flows with particular emphasis on the incompressible Navier-Stokes equation", *Computer Methods in Applied Mechanics and Engineering*, Vol. 32, pp. 199-259.

Codina, R. (1993), "A discontinuity-capturing crosswind – dissipation for the finite element solution of the convection – diffusion equation", *Computer Methods in Applied Mechanics and Engineering*, Vol. 110, pp. 325-42.

Mackenzie, J. and Shuttleworth, R. (1949), "Phenomeno-logical theory of sintering", *Proc. Phys. Soc.*, Loudon, Vol. 62 [12-B], pp. 833-52.

Ming-Shen, Sun, M. and Beaman, J. (1991a), "A three dimensional model for selective laser sintering", *Proceedings of Solid Freform Fabrication Symposium*, Austin, TX, pp. 102-9.

Ming-Shen, Sun, M., Nelson, J., Beaman, J. and Barlow, J. (1991b), "A model for partial viscous sintering", *Proceedings of Solid Freform Fabrication Symposium*, Austin, TX, pp. 46-55.

Papanastasiou, T.C., Malamataris, N. and Ellwood, K. (1992), "A new outflow boundary condition", *International Journal for Numerical Methods in Fluids*, Vol. 14, pp. 587-608.

Scherer, G. (1977a), "Sintering of low density glasses: I, theory", *J. Am. Cer. Soc.*, Vol. 60 No. 5-6, pp. 236-9.

Scherer, G. (1977b)m "Sintering of low density glasses: II, experimental study", *J. Am. Cer. Soc.*, Vol. 60 No. 5-6, pp. 239-45.

Scherer, G. (1977c), "Sintering of low density glasses: III, effect of a distribution of pore size", *J. Am. Cer. Soc.*, Vol. 60 No. 5-6, pp. 245-8.

Scherer, G. (1986), "Viscous sintering under a uniaxial load", *J. Am. Cer. Soc.*, Vol. 69 No. 9, pp. 206-07.

Weissman, E.M. and Hsu, M.B. (1991), "A finite element model of multilayered laser sintered parts", *Proceedings of Solid Freform Fabrication Symposium*, Austin, TX, pp. 86-94.

Williams, J.D. and Deckard C.R. (1998), "Advances in modeling the effects of selected parameters on the SLS process", *Rapid Prototyping Journal*, Vol. 4 No. 2, pp. 90-100.

Yagui, S. and Kunni, D. (1989), "Studies on effective thermal conductivities in packed beds", *J. AIChe.*, Vol. 3 No. 3, pp. 373-81.

**Figure 8** Sintered depth for different scanning speeds for both sets of analysis